Protein Flexibility in Docking-Based Virtual Screening: Discovery of Novel Lymphoid-Specific Tyrosine Phosphatase Inhibitors Using Multiple Crystal Structures

Xuben Hou,[†] Kangshuai Li,[‡] Xiao Yu,[‡] Jin-peng Sun,[§] and Hao Fang*,[†]

[†]Department of Medicinal Chemistry, Key Laboratory of Chemical Biology of Natural Products (MOE), School of Pharmacy,
[‡]Department of Physiology, School of Medicine, and [§]Key Laboratory Experimental Teratology of the Ministry of Education and
Department of Biochemistry and Molecular Biology, School of Medicine, Shandong University, Jinan, Shandong 250012, China

S Supporting Information

ABSTRACT: Incorporating protein flexibility is a major challenge for docking-based virtual screening. With an increasing number of available crystal structures, ensemble docking with multiple protein structures is an efficient approach to deal with protein flexibility. Herein, we report the successful application of a docking-based virtual screen using multiple crystal structures to discover novel inhibitors of lymphoid-specific tyrosine phosphatase (LYP), a potential drug target for autoimmune diseases. The appropriate use of multiple protein structures allowed a better enrichment than a single structure in the recovery of known inhibitors.

Subsequently, an optimal ensemble of LYP structures was selected and used in docking-based virtual screening. Eight novel LYP inhibitors (IC$_{50}$ ranging from 7.95 to 56.6 μM) were identified among 23 hit compounds. Further studies demonstrated that the most active compound **B15** possessed some selectivity over other protein phosphatases and could effectively up-regulate TCR (T cell receptor)-mediated signaling in Jurkat T cells. These novel hits not only provided good starting points for the development of therapeutic agents useful in autoimmune diseases but also demonstrated the advantages of choosing an appropriate ensemble of protein structures in docking-based virtual screening over using a single protein conformation.
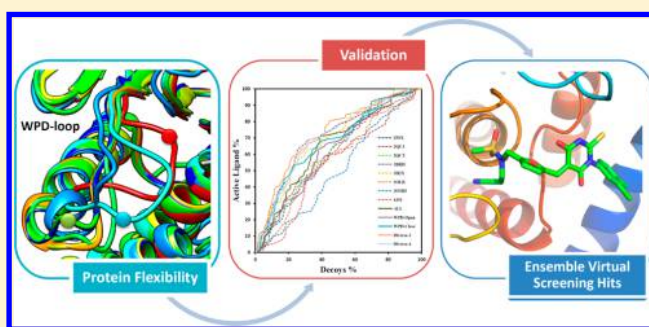
1. INTRODUCTION

Molecular docking is recognized as an indispensable component in drug design and discovery.[1−3] By taking advantage of high-performance computers, docking-based virtual screening is an efficient strategy to identify bioactive compounds and serves as a complementary approach to experimental high-throughput screening (HTS).[4−6] Typically, classical molecular docking programs consist of two parts: (i) prediction of a suitable binding conformation of a ligand to its target protein and (ii) calculation of the binding free energy using the score function.[7] Many docking programs have been developed and applied in docking-based virtual screening such as AutoDock,[8,9] Dock,[10,11] Gold,[12,13] Glide,[14,15] Surflex-dock,[16] FlexX,[17] and VoteDock[18] among others.

Although considerable progress has been achieved in the development of docking algorithms, protein flexibility remains a major challenge in the application of docking-based virtual screening.[19−23] In actual biological systems, both proteins and ligands are flexible entities. The "induced-fit" mode presumes that the protein structure could be induced to the bound conformation when binding to the corresponding ligand.[24−26] So far, ligand flexibility can be handled by various algorithms, but protein flexibility cannot be easily achieved because of the computational cost, which makes it impractical for large-scale

virtual screening. It should be mentioned that even a slight conformational change in the protein binding site would have a notable effect on the calculation of the ligand binding free energy as well as the prediction of favorable binding pose, leading to failure of the molecular docking if this conformational change is not taken into consideration.

The ideal approach to cope with protein flexibility would be to screen all possible conformations of a ligand against the full degrees of freedom of the protein structure, using methods such as molecular dynamics simulations.[27−29] Unfortunately, such an approach is infeasible because of the high cost of computing resources. Consequently, several streamlined methods have been developed to solve this problem, which balances the docking accuracy versus computational cost. Soft docking[30,31] is the earliest solution with a score function that tolerates a certain degree of steric clashes while the protein is still treated as a rigid structure. Several flexible docking programs were developed, in which protein flexibility is limited to a few side chains in the binding sites, making the problem less computationally demanding.[9,21,30] However, these methods still fail to address the backbone movement or other major
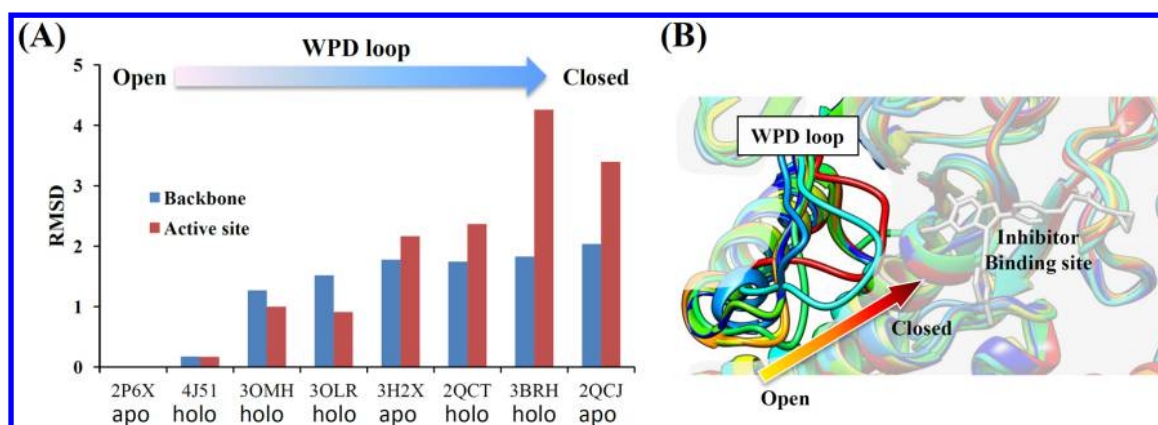
Figure 1. Comparison of LYP crystal structures. (A) RMSD values of the C-α backbone and active site residues of eight LYP structures. 2P6X is used as the reference structure. (B) Superposition of eight LYP structures: 2P6X (green), 4J51 (blue), 3OLR (orange), 3OMH (yellow), 3H2X (cornflower blue), 2QCT (forest green), 3BRH (red), 2QCJ (cyan).
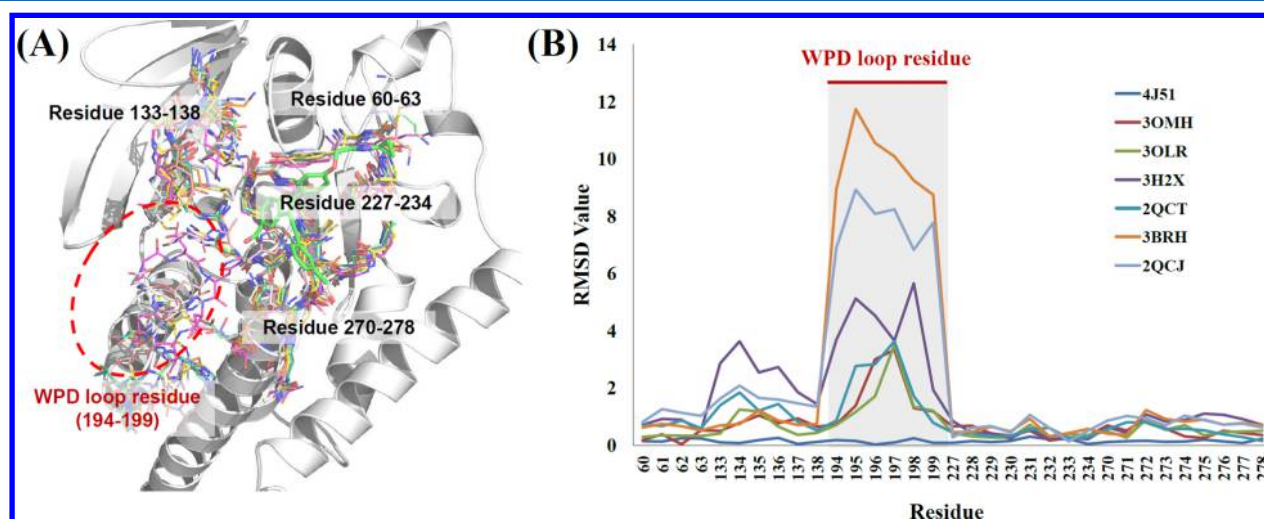

Figure 2. (A) Comparison of active site residues of eight LYP crystal structures. Protein structure (PDB: 4J51) is shown in cartoon, and the cocrystal inhibitor **8b** is colored in green. (B) RMSD values for each residue in the active site. 2P6X is used as the reference structure.

structural rearrangements of the target proteins where the full flexibility of the protein should be taken into consideration in the docking calculation. One method to account for protein flexibility is to dock ligands to multiple conformations of the protein, commonly referred as "ensemble docking".[31−33] Recent studies have already shown that the use of multiple protein structures could be beneficial in both pose prediction and virtual screening.[31,34−37] With the development of structural biology, the numerous crystal structures in the protein data bank (PDB) provide good sources of multiple protein conformations. It follows that one of the most challenging questions to harness the information contained in multiple protein structures is how to efficiently combine the various protein structures for ensemble docking.[38] Based on this observation, we investigated the possibility of developing a docking-based ensemble virtual screening method based on multiple crystal structures using lymphoid-specific tyrosine phosphatase (LYP), a member of the protein tyrosine phosphatases (PTPs) family,[39] as a trial example.

Encoded by the *PTPN22* gene, LYP is an important regulator of T-cell receptor (TCR) signaling pathways and is the subject of intensive research.[40] Genetic studies revealed that a classical missense C1858T polymorphism in the *PTNP22* gene serves as a common risk factor for many autoimmune diseases.[41] The encoded gene product has a Trp at position 620 instead of an Arg (R620W). The LYP-R620W variant was shown to have a diminished interaction with the SH3 domain of Csk,[42] which potentiates the inhibitory activity of LYP in T cell signaling and makes this variant an important pathogenic factor in autoimmune disorders.[43] Although the mechanism of the LYP-R620W variant in autoimmunity still remains unclear, functional studies have demonstrated that this variant is a gain-of-function mutant.[44,45] Therefore, a specific LYP inhibitor has great therapeutic potential for autoimmune diseases, especially for patients carrying the W620 polymorphism.[46] Considering the fact that most small molecular LYP inhibitors discovered to date are highly charged carboxylic acid derivatives, non-carboxylic acid-containing ligands would be highly desirable for improving the overall drug-like properties of the inhibitor.[47] Our previous study reported a noncarboxylic acid-containing LYP inhibitor, **A19**, which could selectively block LYP activity at the cellular level.[43] Heretofore, a total of 8 crystal structures of LYP with or without inhibitors have been determined. Therefore, virtual screening using these X-ray crystallographic structures was initiated to explore the impact of protein flexibility in the *in silico* discovery of LYP inhibitors.

In the present study, we reported the successful application of docking-based virtual screening based on multiple crystal
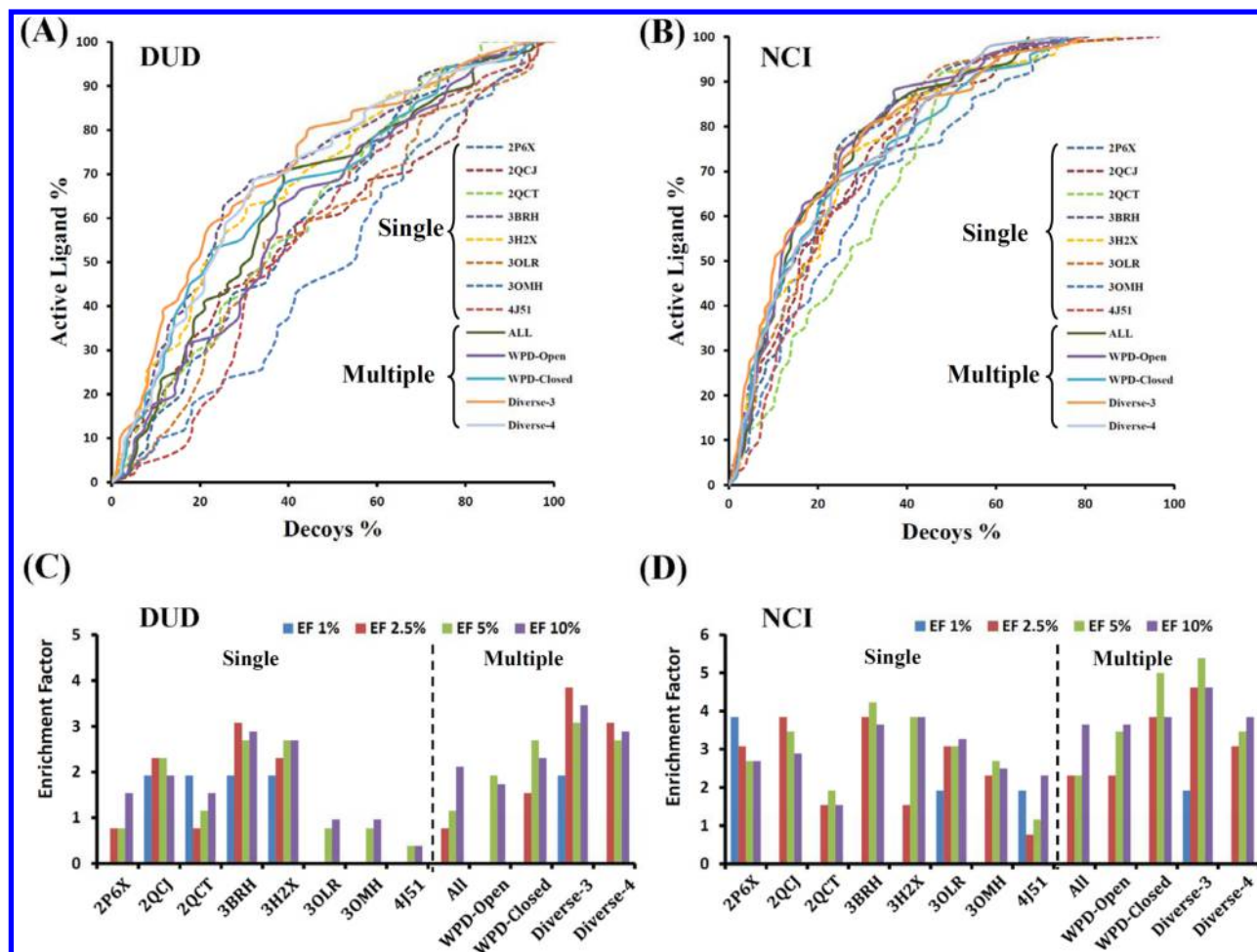
Figure 3. Validation of virtual screening based on single or multiple crystal structures using the DUD database and NCI database. (A) Roc plots for the DUD database. (B) Roc plots for the NCI database. (C) Enrichment factors for the DUD database. (D) Enrichment factors for the NCI database.

structures for the discovery of LYP inhibitors. The accuracy of ensemble virtual screening was evaluated by the recovery of known ligands from decoy compounds. The optimal ensemble of structures was determined and employed in docking-based virtual screening of a commercial database for identification of noncarboxylic acid-containing LYP inhibitors.

2. RESULTS

2.1. Analysis of the Protein Flexibility of LYP. So far, eight LYP crystal structures have been determined (Supporting Information, Table S1). To analyze the protein flexibility, all available crystal structures were superimposed using 2P6X as the reference structure (Figure S1 in the Supporting Information) as well as the resulting root-mean square deviations (RMSD) values for both backbone structure and active site residues (Figure 1A). A visual inspection focusing on the binding site of the aligned structures revealed the most striking difference among all the structural residues is the conformation of the Trp-Pro-Asp (WPD, residues 193−204) loop. The diverse conformations of the WPD loop are shown in Figure 1B. We further compared the residues in active site of eight LYP crystal structures and calculated the RMSD values for each amino acid residues. Results further proved that the flexibility of the WPD loop residues contributes most to the differences in the active site of LYP (Figure 2).

As mentioned elsewhere, the conserved WPD loop of LYP plays an important role in the catalyzing tyrosine dephosphorylation, especially for substrate/inhibitor recognition.[46,48−50] In previously determined crystal structures of LYP, the WPD loop could be found in either a "closed" conformation or an "open" conformation. In the LYP-inhibitor complex (e.g., PDB codes 4J51 and 2QCT), the WPD loop shifts to the outer side of the active site to accommodate the binding of inhibitor, presenting an "open" conformation. However, diverse conformations of the WPD loop were observed when bound with different substrate-related peptides (e.g., PDB codes 3OLR, 3OMH, and 3BRH). In terms of the apo-LYP crystal structures, the WPD loop can be observed in either the "closed" conformation (e.g., PDB code 2QCJ) or the "open" conformation (e.g., PDB codes 2P6X and 3H2X). This structural information confirmed the flexibility of the WPD loop and considering its importance in inhibitor reorganization, we constructed a docking-based virtual screening platform for LYP inhibitors using multiple crystal structures.

2.2. Validation of Ensemble Virtual Screening. The major challenge of virtual screening using multiple protein structures is to efficiently combine all available protein structures. First, we combined all eight LYP crystal structures (PDB codes 2P6X, 2QCJ, 2QCT, 3BRH, 3H2X, 3OLR, 3OMH, and 4J51) to make full use of all available structural

information. Then, we combined the structures with "open" WPD loops (PDB codes 2P6X, 3OLR, 3OMH, 3H2X, and 4J51) and "closed" WPD loops (PDB codes 2QCT, 3BRH, and 2QCJ). Additionally, we selected several crystal structures based on the RMSD values in Figure 1A to represent diverse conformations of the WPD loop. As suggested by a previous study, approximately 2−5 protein structures are enough for the ensemble virtual screening,[51,52] balancing the docking accuracy and computational cost. Thus, three (Diverse-3, PDB codes 2P6X, 3BRH, and 2QCJ) or four (Diverse-4, PDB codes 2P6X, 2QCT, 3BRH, and 2QCJ) crystal structures were also selected for ensemble virtual screening, based on the RMSD values of backbone and active site residues and visual inspection of the WPD loop (Figure 1). Finally, a total of five different combinations of the LYP crystal structures were used in the ensemble virtual screening.

The discriminatory power of the ensemble virtual screening was then evaluated by screening the validation database containing known LYP inhibitors and confusing decoys. Two different decoys sets (DUD database[53,54] and NCI database[55,56]) were used in the validation, so as to obtain an unbiased performance of the enrichment. The molecular docking program Gold and the GoldScore[13] were used in the present docking-based virtual screening based on a previous study.[43] The Redock study was performed using the LYP-**8b** cocrystal structure (PDB code 4J51) employing four different docking modes of GOLD (*Library Screening, Virtual Screening, Default,* and *Very Flexible*). Results indicated that the docking parameters of the *Default* mode is good enough to predict the correct binding pose of **8b** (Figure S2 in the Supporting Information). Consider the docking accuracy and time-consuming, the default docking parameters of GOLD were employed in the current study. In addition to ensemble approaches, we also evaluated the docking-based virtual screening using single protein structures separately. The ROC plots and calculated enrichment factor (EF) at 1%, 2.5%, 5%, and 10% are shown in Figure 3. The overall AUC values and AUC values for top 10% screened database were also calculated, and results are summarized in Table 1.

As shown in Figure 3, the different performances obtained from virtual screening using single protein structures further corroborated the impact of protein flexibility in docking-based virtual screening. Among the eight LYP crystal structures,

3BRH exhibited better performance than the others from both the DUD database and NCI database. We also found that the discriminating powers of single protein structures are not in line with their structure resolutions. Comparison of the result from ensemble virtual screening to single protein virtual screening shows that the discriminatory power could be improved when the protein structures were properly combined. The combination of Diverse-3 resulted in the highest EF values and AUC values in the two validation databases. However, the more complex combination (Diverse-4) did not help to increase the virtual screening enrichment, possibly because of the bad performance of 2QCT in the single protein virtual screening. We also analyzed the number of top-scored known LYP inhibitors for each crystal structure (Supporting Information, Figure S3) and found that 2P6X, 2QCJ, and 3BRH possessed a larger number of top-scored hits than other crystal structures, which might explain the good performance of the Diverse-3 ensemble. When all eight crystal structures were used in the ensemble virtual screening, the enrichment did not increase in either validation databases. Furthermore, the combination of WPD-closed structures showed a better performance than that of the WPD-open structures. Although the two validation databases contain a different number of confusing decoys, we obtained a similar performance for each single structure and ensemble protein structures in the two different databases. So the size of the database did not bias the results of our validation. Therefore, we concluded that virtual screening based on multiple crystal structures could achieve higher discriminatory power than the data using single crystal structure, and the selection of crystal structures for the ensemble is critical for good performance. In the current case, the ensemble virtual screening using 2P6X, 3BRH, and 2QCJ possesses high sensitivity to known LYP inhibitors.

2.3. Virtual Screening of LYP Inhibitors Based on Multiple Crystal Structures. Because the ensemble virtual screening using multiple crystal structures yielded high enrichment factors for the recovery of known LYP inhibitors, we sought to apply the approach in discovery of novel LYP inhibitors. The ensemble virtual screening was carried out following the workflow described in Figure 4. As noncarboxylic acid-containing ligands are highly desirable for the development of LYP inhibitors, we first filtered the commercial SPECS database and excluded 6,697 compounds that contained the carboxylic acid groups. Then all the remaining compounds were each docked to the three selected LYP structures (PDB codes 2P6X, 2QCJ, and 3BRH) using GOLD 5.0 and ranked based on the highest GoldScores among the three crystal structures. After deleting duplicate structures, a total of 1324 hits were selected for cluster analysis, in which the hit compounds were divided into 10 groups according to their structural features. Finally, a visual inspection was further performed, and 23 hits were identified for further biological evaluation.

The inhibitory activities of the 23 purchased compounds were tested based on the inhibition of LYP-catalyzed hydrolysis of pNPP. These hit compounds were initially screened at 100 μM, and for compounds that showed more than 50% inhibition, we further determined their concentration-dependent inhibition. Finally, compounds **B1, B2, B4, B5, B11, B15, B16,** and **B23** were found to be active with $IC_{50} < 60$ μM (Table 2). Remarkably, compound **B15** had a similar potency ($IC_{50} = 7.9$ μM) compared with the previously reported inhibitor **I-C11**[46] ($IC_{50} = 4.6$ μM) and **A15**[43] ($IC_{50} = 6.1$ μM). Interestingly, the highest GoldScore of these newly identified

Table 1. AUC Values of Virtual Screening Using Single or Multiple Crystal Structures

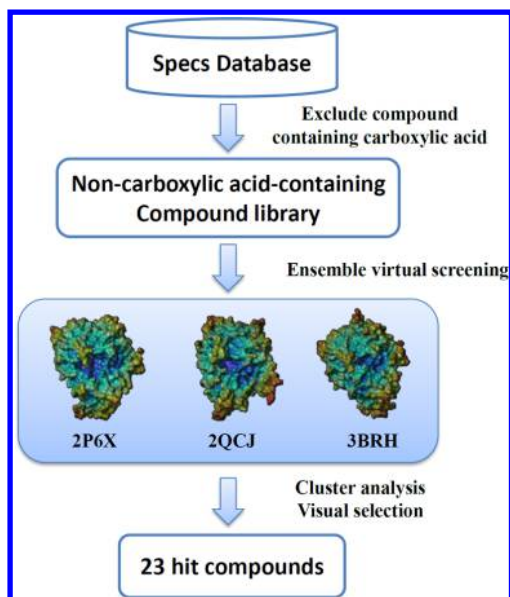| method	crystal structure(s)	DUD database		NCI database	
		AUC	AUC$_{10\%}$	AUC	AUC$_{10\%}$
single	2P6X	0.61	0.06	0.80	0.18
	2QCJ	0.58	0.12	0.78	0.18
	2QCT	0.63	0.07	0.72	0.11
	3BRH	0.71	0.14	0.78	0.21
	3H2X	0.69	0.14	0.78	0.21
	3OLR	0.57	0.04	0.80	0.20
	3OMH	0.50	0.04	0.73	0.12
	4J51	0.57	0.04	0.76	0.10
multiple	all	0.65	0.08	0.80	0.18
	WPD-open	0.62	0.07	0.81	0.19
	WPD-closed	0.67	0.12	0.78	0.22
	Diverse-3	**0.72**	**0.17**	**0.82**	**0.26**
	Diverse-4	0.70	0.14	0.78	0.21

Figure 4. Protocol for ensemble virtual screening of LYP inhibitors.

inhibitors were derived from different crystal structures. These results further revealed the advantages of incorporating protein flexibility in docking-based virtual screening by using multiple crystal structures rather than a single structure.

2.4. Structural Analysis and Predicted Binding Patterns of Potent Inhibitors. The novelty of the eight active compounds with respect to existing LYP inhibitors were evaluated by calculating Tanimoto similarity values (T) based on the FCFP_4 fingerprints.[57] According to a previous study,[58] structures with a T value higher than 0.85 could be considered as similar. As shown in Table S2 (Supporting Information), all these newly identified inhibitors can be considered to be structurally novel with T values less than 0.22. The ADMET-based profile for the active compounds were calculated as well as the LogP values. Results indicated that these newly identified inhibitors, especially the most active compound **B15**, possessed similar pharmacokinetic and toxicity properties with known inhibitor **8b** (Table S3 in the Supporting Information). We further analyzed the chemical structures of eight newly identified inhibitors using the list of pan assay interference compounds (PAINs).[59] Compounds **B1**, **B11**, and **B23** could pass the PAINS filter, whereas other compounds have possible problematic substructures such as rhodanine (compounds **B2**, **B4**, **B5**, and **B16**) and barbiturate (compound **B15**). It should be mentioned that previous studies have proved that different chemical modifications could lead to changes in promiscuity effects.[60−62] So these newly indentified LYP inhibitors provided valuable starting points for the further structure optimizations to improve both activity and selectivity.

Figure 5 shows the predicted binding mode of compounds **B5**, **B11**, and **B15** (IC$_{50}$ < 20 μM) to the top-scored protein structures, as well as the binding interactions of known inhibitor **8b** in the cocrystal structure (PDB code 4J51). Hydrogen bond interactions are one of the most common ligand-target interactions. As proposed in Figure 5, all of these three inhibitors could bind to the LYP active site and form multiple hydrogen bond interactions with residues around the binding site (Arg233 and Gln274 for **B5**; Tyr60, Cys231, Arg233, and Gln274 for **B11**; Asp62, His196, Ser228, Ala229, Arg233, Gln274, and Gln278 for **B15**). The eight hydrogen

bonds may explain the higher inhibitory activity of compound **B15** than that of compounds **B5** and **B11**. The binding mode of compound **B15** is similar to that of **8b**. Additionally, $\pi-\pi$ stacking interactions could be observed between Tyr 60 and these three compounds.

To further analyze the effect of the WPD loop in the docking study of the LYP inhibitor, we checked the predicted binding poses of compound **B15** in three crystal structures of Diverse-3 ensemble (2P6X, 2QCJ, and 3BRH). As shown in Figure S4 in the Supporting Information, the flexibility of the WPD loop, especially the different conformations of residue His196, resulted in different binding modes of compound **B15**. The active site is either too big (in 2P6X) or too small (in 2QCJ) to accommodate the binding of compound **B15**, whereas the active site in 3BRH is more suitable. The predicted hydrogen bond interaction between His196 and compound **B15** (Figure 5C) also demonstrated the importance of this residue. These results are helpful to understand the higher docking score of compound **B15** in 3BRH than that in 2P6X and 2QCJ.
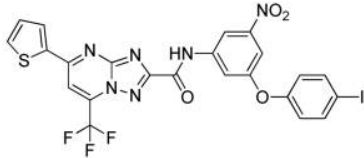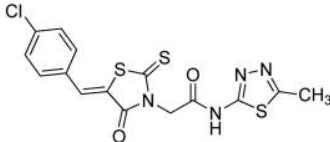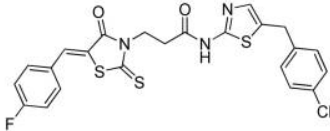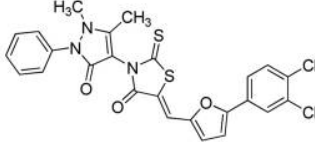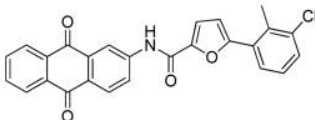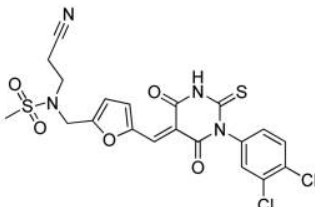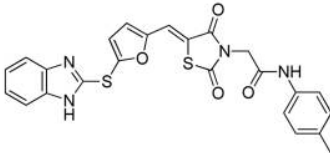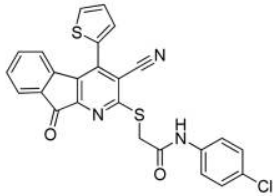
2.5. Selectivity toward Other Protein Phosphatases of B15. Considering the fact that active sites of all classical tyrosine phosphatases are very similar, the selectivity of a LYP inhibitor is an important factor for biological and clinical usage.[63,64] Therefore, we evaluated the selectivity of the most potent compound **B15** against a panel of protein phosphatases, including PTP1B, VHR, STEP, PTPN18, Glepp, Slingshot2, PPM1A, PPM1G, and PP1. As shown in Figure 5A, compound **B15** possessed approximately 1.2−12-fold selectivity for LYP over other protein phosphatases (Figure 6A).

A previous study has reported that the flexibilities of WPD loops could be observed in many other PTPs family members and is also of paramount importance for the development of selective PTP inhibitors.[65] Among the nine protein phosphatases tested in our study, compound **B15** showed good selectivity for LYP over most protein phosphatases that do not belong to the PTPs family (SSH2, PPM1A, PPM1G, and PP1), except for VHR. In terms of selectivity of compound **B15** for PTPs family members (LYP, PEST, STEP, and PTPN18), the structure differences in their WPD loops may be helpful in understanding the selectivity profile of compound **B15**. For example, the absence of residue His196 in the WPD loop of STEP and PTPN18 may explain the lower activities of compound **B15** for STEP and PTPN18 than that for LYP, because *in silico* results suggested the importance of His196 in the binding of compound **B15** to LYP (Figure 4C and Supporting Information Figure S4). Although the crystal structure of PEST has not been determined, high similarity in their sequences may explain the low selectivity of compound **B15** for LYP over PEST.

2.6. Effect of B15 on the ERK Phosphorylation. Because compound **B15** is a potent LYP inhibitor and possesses a certain degree of selectivity, we further evaluated its effect on TCR signaling using the Jurkat T antigen (JTAg) human T cell line. Previous studies have demonstrated that LYP could down-regulate the phosphorylation level of ERK after TCR activation.[43,46] Thus, the phosphorylation levels of ERK should increase when the activity of LYP was blocked by an inhibitor. The activation of the TCR was induced by the anti-CD3 (OKT) antibody. After incubation with the inhibitor **B15** at 20 μM, the phosphorylation level of ERK (pT202 and pY204) was significantly increased (Figure 6B).

2.7. Insight into the Binding of B15 to LYP. To further explore the structural basis for the binding of **B15** to LYP, we

Table 2. Chemical Structures, Inhibitory Activities, GoldScore, and Top-Scored Crystal Structures of Eight Active Compounds

Name	Structure	$IC_{50}(\mu M)$	GoldScore	Top-score crystal structure
B1		49.3±12.6	70.89	3BRH
B2		56.6±10.5	60.23	2QCJ
B4		44.3±13.2	72.71	3BRH
B5		13.6±3.8	66.45	2QCJ
B11		13.8±6.9	64.82	2P6X
B15		**7.95±0.2**	64.54	3BRH
B16		24.3±4.1	75.44	3BRH
B23		40.9±9.3	69.64	2P6X

performed a 20 ns molecular dynamics simulation using the LYP-**B15** complex predicted by molecular docking (Figure 5C). The stability of the LYP-**B15** complex was evaluated by calculating the root-mean-square deviation (RMSD) values of the protein backbone structure and inhibitor **B15** during simulation. Results in Figure 7 showed that the conformation of

the LYP-**B15** complex stabilized after approximately 2 ns of simulation. Compound **B15** remains in the binding pocket, and only slight movements were observed during the simulation (Figure 7B and Video S1). We also detected the hydrogen bond interactions between **B15** and residues in binding pocket (Video S2). All these molecular dynamics results were
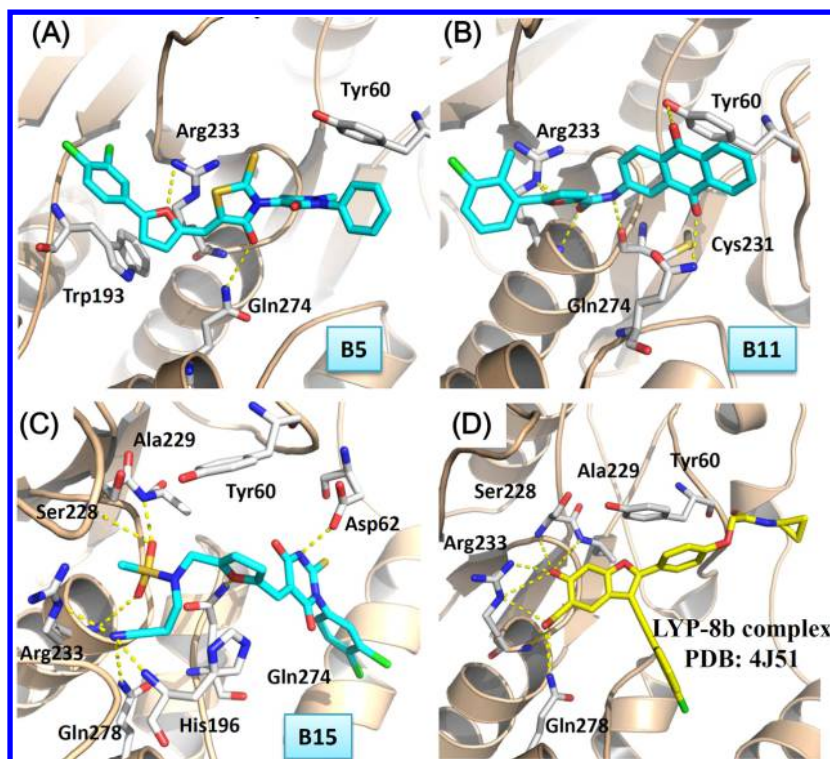
Figure 5. Top-scored conformations of compounds **B5**, **B11**, and **B15** and target-ligand interactions of known LYP inhibitor **8b** in cocrystal structure. (A) Predicted binding mode of compound **B5** docked to protein structure 2QCJ; (B) Predicted binding mode of compound **B11** docked to protein structure 2P6X; (C) Predicted binding mode of compound **B15** docked to protein structure 3BRH. (D) Binding interactions of inhibitor **8b** in crystal structure 4J51.
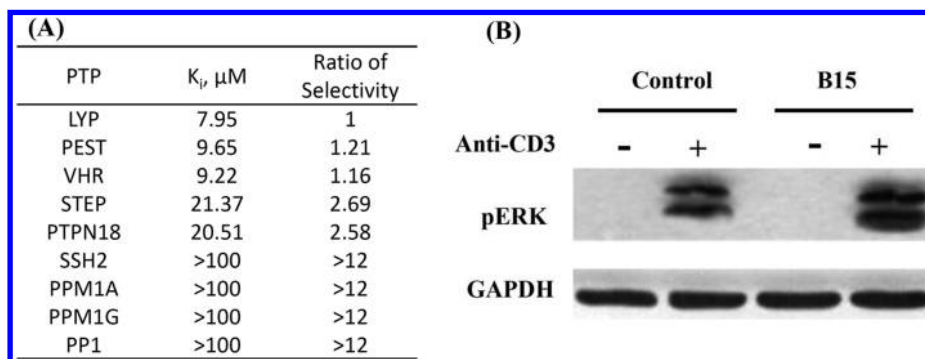

(A)

PTP	K_i, μM	Ratio of Selectivity
LYP	7.95	1
PEST	9.65	1.21
VHR	9.22	1.16
STEP	21.37	2.69
PTPN18	20.51	2.58
SSH2	>100	>12
PPM1A	>100	>12
PPM1G	>100	>12
PP1	>100	>12

Figure 6. (A) Selectivity of compound **B15** for a panel of protein phosphatases. (B) Effects of **B15** on the anti-CD3 (OKT) induced phosphorylation of ERK pT202 and pY204 as detected by a phosphorylation-specific antibody. The GAPDH level was used as a control.

beneficial for the understanding of the inhibition mechanism of compound **B15** against LYP.

3. CONCLUSION

We describe the development and application of an ensemble virtual screening strategy for LYP inhibitors. Combining the use of three LYP crystal structures with different conformations of the WPD loop proved to be helpful to deal with protein flexibility and improve the performance of docking-based virtual screening. After a multistage virtual screening protocol, 23 hit compounds were selected and tested *in vitro* against LYP, which led to the identification of eight micromolar (from 7.95 μM to 56.6 μM) LYP inhibitors with novel chemotypes. Further exploration demonstrated that the most active compound **B15** possessed a certain degree of selectivity over a panel of other protein phosphates. We also confirmed that

B15 is a cell-permeable LYP inhibitor that could up-regulate the TCR-induced phosphorylation of ERK in Jurkat T cells.

In summary, these newly identified LYP inhibitors not only confirmed the successful application of ensemble virtual screening using properly selected crystal structures but also provided novel noncarboxylic acid-containing scaffolds bearing LYP inhibitory activities.

4. MATERIALS AND METHODS

4.1. Materials. The selected virtual screening hits were purchased from SPECS with purities confirmed by LC-MS and ^{1}H NMR (data available at http://www.specs.net/). The *p*-nitrophenyl phosphate (pNPP, 4264-83-9) was purchased from Sangon Biotech Co., Ltd. Ni-NTA agarose was obtained from Amersham Pharmacia Biotech. The ERKpT[202]/pY[204] antibodies were obtained from Cell Signaling Technology. The anti-CD3
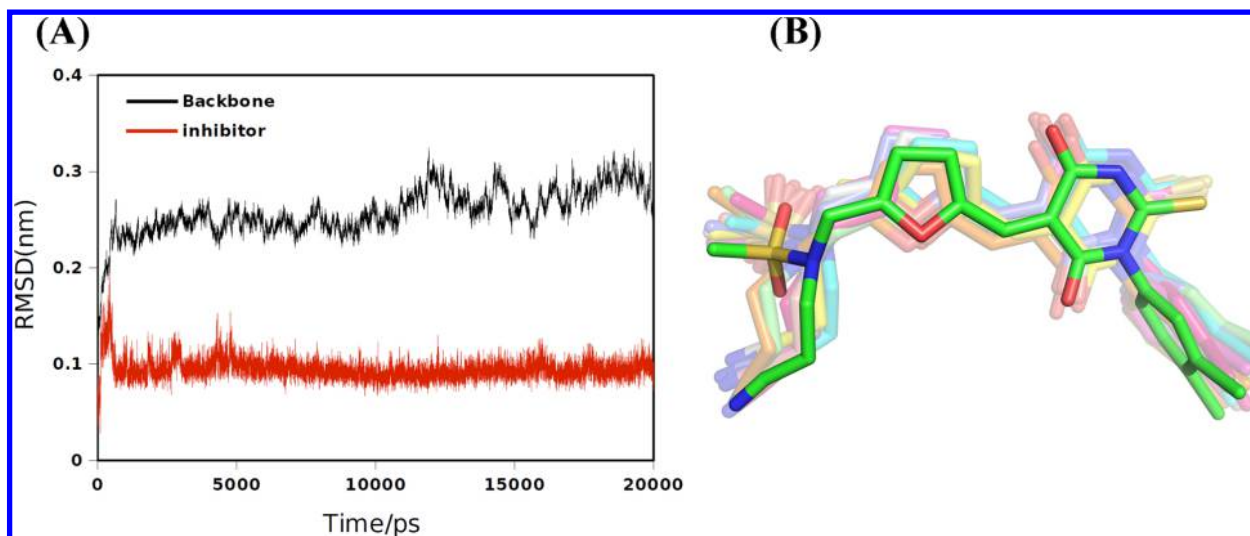
Figure 7. (A) RMSD plots of LYP backbone structure and inhibitor **B15** during the 20 ns molecular dynamics simulation. (B) Trajectory overlay of **B15** over the simulation.

(OKT3) was purchased from eBioscience. The mouse anti-GAPDH monoclonal antibody was obtained from ZSGB-BIO Co. All other chemicals and reagents were purchased from Sigma.

4.2. Preparation of Receptor Structures. Eight crystal structures of LYP were retrieved from the Protein Data Bank: PDB codes 2P6X, 2QCT, 2QCJ, 3BRH, 3H2X, 3OLR, 3OMH, and 4J51. Each crystal structure was prepared using the protein preparation workflow in Sybyl-x 1.1 (Tripos, Inc.). Missing atoms and hydrogen atoms were added, and all water molecules, metal ions, and small chemical groups were removed. AMBER FF99 partial charge was assigned to each protein structure. The mutated residues were changed back using Discovery Studio 2.5. Alignment and comparison of these crystal structures were performed using *Align Structures by Homology* module of Sybyl-x 1.1.

4.3. Validation Databases and Evaluation Methods. Two different validation databases were constructed by mixing 55 reported LYP inhibitors[42,43,45,66] with the NCI database[55,56] and the Discovery of Decoys (DUD) database.[53,54] It should be mentioned that only the structure of the most active LYP inhibitor **8b** was derived from the cocrystal structure 4J51 so the statistic results will not be influenced when this single compound was mixed with 54 other structurally diverse LYP inhibitors. The mix of active compounds with decoys provided an efficient validation database to evaluate the discriminating abilities of different virtual screening methods. The NCI database contains 1,895 compounds with diverse structures, and the DUD database contains 2,950 bioactive compounds with activity against 40 targets. As mentioned in our previous study, the DUD database is stricter than the NCI Diverset because the DUD database contains a larger number of bioactive compounds and it is more difficult to discriminate LYP inhibitors from known bioactive compounds for other targets.[43] Virtual screening of the two validation databases was performed using Gold 5.0 and GoldScore, which showed high sensitivity to LYP inhibitors in our previous investigation.[43] Both single protein structure-based and multiple structure-based virtual screening were performed using the default parameter of Gold. Virtual screening results were ranked based on GoldScore values. For results of virtual screening using

multiple crystal structures, the highest GoldScore among different crystal structures was selected for each compound. Enrichment factors (EF) at 1%, 2.5%, 5%, and 10% of the screened database were calculated according to eq 1

$$EF = \frac{N_{experimental}^{x\%}}{N_{expected}^{x\%}} = \frac{N_{experimental}^{x\%}}{N_{active \cdot x\%}^{x\%}} \tag{1}$$

where $N_{experimental}$ = number of experimentally found active structures in the top x% of the sorted database, $N_{expected}$ = number of expected active structures, and N_{active} = total number of active hits in database.

Additionally, we also calculated the AUC (Area Under roc Curve) values using GraphPad Prism 6 to assess the overall performance of the virtual screening.

4.4. Database Preparation and Ensemble Virtual Screening. Ligprep (Schrodinger, Inc.) was used in the ligand preparation of the SPCES database. Additionally, the ionization state of each compound was generated using the Ionizer program. Then, compounds containing carboxylic acid groups were excluded to generate the noncarboxylic acid containing database for subsequent virtual screening of novel LYP inhibitors. A combination of three crystal structures (PDB codes 2QCJ, 2P6X, and 3BRH) was used for ensemble virtual screening. The docking program GOLD 5.0 was used with the critical parameters set to the default values. Finally, the selected top-ranking compounds were clustered based on the FCFP_6 fingerprints calculation and then selected manually.

4.5. Molecular Dynamics. Molecular dynamics simulations were performed using GROMACS 4.5.2,[67,68] with the AMBER99SB-ILDN force field[69] and the TIP3P water model.[70] The starting ligand pose of **B15** was taken from the molecular docking result using GOLD. The Particle Mesh Ewald (PME)[71] method was used to deal with long-range electrostatics interactions, and all bonds containing hydrogen atoms were fixed by the P-LINCS[72] algorithm. The topology file for compound **B15** was generated using Antechamber[73,74] and the AmberTools package with the partial charges assigned using the AM1-BCC[75,76] method in USCF Chimera.[77] The 20 ns molecular dynamics simulation was carried out following the procedure described in a previous study.[78]

4.6. Protein Expression, Purification, and IC$_{50}$ Measurements. The expression and purification of the LYP catalytic domain (residues 1−294) as well as other protein phosphatases were performed as described previously.[79−84] The effect of small molecule inhibitors on the PTP-catalyzed pNPP hydrolysis were determined at 25 °C in 50 mM 3,3-dimethylglutarate buffer, and the ionic strength was adjusted to 0.15 M with NaCl (buffer A). The reaction was quenched at set time points using 1 M NaOH, and the generation of products was detected by monitoring the absorbance of pNP at 405 nm. The IC$_{50}$ value was calculated by GraphPad Prism using the following equation:

$$v = V_{max}*IC_{50}/(IC_{50} + [S])$$

4.7. Western Blotting. The human Jurkat T cells (purchased from the ATCC) were grown at 37 °C in RPMI 1640 medium supplemented with 10% FBS as previously described.[79,80] The Jurkat T cells were preincubated with a small molecule inhibitor (20 μM) or DMSO for 1 h. Then, the cells were stimulated with 5 μg/mL anti-CD3 antibody (OKT3) or medium for 5 min and then lysed in lysis buffer (50 mM Tris, pH 7.5, 150 mM NaCl, 10 mM NaF, 2 mM EDTA, 10% glycerol, 1% NP-40, 0.25% sodium deoxycholate, 1 mM NaVO$_4$, and protease cocktail). The protein concentrations of the lysates were measured using the BCA Protein Quantitation Kit (Beyotime). Equal amounts of each cell lysate were denatured in 2×SDS loading buffer and boiled for 10 min. The protein samples were then subjected to Western blotting.

■ ASSOCIATED CONTENT

Ⓢ Supporting Information

The Supporting Information is available free of charge on the ACS Publications website at DOI: 10.1021/acs.jcim.5b00344.

Figures S1−S4 and Tables S1−S3 (PDF)

LYP: Compound **B15** (MPG)

Hydrogen bond interactions between **B15** and residues in the binding pocket (MPG)

■ AUTHOR INFORMATION

Corresponding Author

*Phone: 86-531-88382731. Fax: 86-531-88382548. E-mail: haofangcn@sdu.edu.cn.

Notes

The authors declare no competing financial interest.

■ ACKNOWLEDGMENTS

■ REFERENCES

(1) Brooijmans, N.; Kuntz, I. D. Molecular Recognition and Docking Algorithms. *Annu. Rev. Biophys. Biomol. Struct.* **2003**, *32*, 335−373.

(2) Hermann, J. C.; Marti-Arbona, R.; Fedorov, A. A.; Fedorov, E.; Almo, S. C.; Shoichet, B. K.; Raushel, F. M. Structure-Based Activity Prediction for an Enzyme of Unknown Function. *Nature* **2007**, *448*, 775−779.

(3) Chen, Y. C. Beware of Docking! *Trends Pharmacol. Sci.* **2015**, *36*, 78−95.

(4) Shoichet, B. K. Virtual Screening of Chemical Libraries. *Nature* **2004**, *432*, 862−865.

(5) Zhuang, C. L.; Narayanapillai, S.; Zhang, W. N.; Sham, Y. Y.; Xing, C. G. Rapid Identification of Keap1-Nrf2 Small-Molecule Inhibitors through Structure-Based Virtual Screening and Hit-Based Substructure Search. *J. Med. Chem.* **2014**, *57*, 1121−1126.

(6) Ripphausen, P.; Nisius, B.; Peltason, L.; Bajorath, J. Quo Vadis, Virtual Screening? A Comprehensive Survey of Prospective Applications. *J. Med. Chem.* **2010**, *53*, 8461−8467.

(7) Hou, X. B.; Du, J. T.; Zhang, J.; Du, L. P.; Fang, H.; Li, M. Y. How to Improve Docking Accuracy of Autodock4.2: A Case Study Using Different Electrostatic Potentials. *J. Chem. Inf. Model.* **2013**, *53*, 188−200.

(8) Santos-Martins, D.; Forli, S.; Ramos, M. J.; Olson, A. J. Autodock4(Zn): An Improved Autodock Force Field for Small-Molecule Docking to Zinc Metalloproteins. *J. Chem. Inf. Model.* **2014**, *54*, 2371−2379.

(9) Morris, G. M.; Huey, R.; Lindstrom, W.; Sanner, M. F.; Belew, R. K.; Goodsell, D. S.; Olson, A. J. Autodock4 and Autodocktools4: Automated Docking with Selective Receptor Flexibility. *J. Comput. Chem.* **2009**, *30*, 2785−2791.

(10) Lang, P. T.; Brozell, S. R.; Mukherjee, S.; Pettersen, E. F.; Meng, E. C.; Thomas, V.; Rizzo, R. C.; Case, D. A.; James, T. L.; Kuntz, I. D. Dock 6: Combining Techniques to Model Rna-Small Molecule Complexes. *RNA* **2009**, *15*, 1219−1230.

(11) Moustakas, D. T.; Lang, P. T.; Pegg, S.; Pettersen, E.; Kuntz, I. D.; Brooijmans, N.; Rizzo, R. C. Development and Validation of a Modular, Extensible Docking Program: Dock 5. *J. Comput.-Aided Mol. Des.* **2006**, *20*, 601−619.

(12) Verdonk, M. L.; Chessari, G.; Cole, J. C.; Hartshorn, M. J.; Murray, C. W.; Nissink, J. W. M.; Taylor, R. D.; Taylor-, R. Modeling Water Molecules in Protein-Ligand Docking Using Gold. *J. Med. Chem.* **2005**, *48*, 6504−6515.

(13) Verdonk, M. L.; Cole, J. C.; Hartshorn, M. J.; Murray, C. W.; Taylor, R. D. Improved Protein-Ligand Docking Using Gold. *Proteins: Struct., Funct., Genet.* **2003**, *52*, 609−623.

(14) Friesner, R. A.; Banks, J. L.; Murphy, R. B.; Halgren, T. A.; Klicic, J. J.; Mainz, D. T.; Repasky, M. P.; Knoll, E. H.; Shelley, M.; Perry, J. K.; Shaw, D. E.; Francis, P.; Shenkin, P. S. Glide: A New Approach for Rapid, Accurate Docking and Scoring. 1. Method and Assessment of Docking Accuracy. *J. Med. Chem.* **2004**, *47*, 1739−1749.

(15) Halgren, T. A.; Murphy, R. B.; Friesner, R. A.; Beard, H. S.; Frye, L. L.; Pollard, W. T.; Banks, J. L. Glide: A New Approach for Rapid, Accurate Docking and Scoring. 2. Enrichment Factors in Database Screening. *J. Med. Chem.* **2004**, *47*, 1750−1759.

(16) Jain, A. N. Surflex-Dock 2.1: Robust Performance from Ligand Energetic Modeling, Ring Flexibility, and Knowledge-Based Search. *J. Comput.-Aided Mol. Des.* **2007**, *21*, 281−306.

(17) Kramer, B.; Rarey, M.; Lengauer, T. Evaluation of the Flexx Incremental Construction Algorithm for Protein-Ligand Docking. *Proteins: Struct., Funct., Genet.* **1999**, *37*, 228−241.

(18) Plewczynski, D.; Lazniewski, M.; Von Grotthuss, M.; Rychlewski, L.; Ginalski, K. Votedock: Consensus Docking Method for Prediction of Protein-Ligand Interactions. *J. Comput. Chem.* **2011**, *32*, 568−581.

(19) Cavasotto, C. N.; Abagyan, R. A. Protein Flexibility in Ligand Docking and Virtual Screening to Protein Kinases. *J. Mol. Biol.* **2004**, *337*, 209−225.

(20) B-Rao, C.; Subramanian, J.; Sharma, S. D. Managing Protein Flexibility in Docking and Its Applications. *Drug Discovery Today* **2009**, *14*, 394−400.

(21) Therrien, E.; Weill, N.; Tomberg, A.; Corbeil, C. R.; Lee, D.; Moitessier, N. Docking Ligands into Flexible and Solvated Macromolecules. 7. Impact of Protein Flexibility and Water Molecules on

Docking-Based Virtual Screening Accuracy. *J. Chem. Inf. Model.* **2014**, *54*, 3198−3210.

(22) Fischer, M.; Coleman, R. G.; Fraser, J. S.; Shoichet, B. K. Incorporation of Protein Flexibility and Conformational Energy Penalties in Docking Screens to Improve Ligand Discovery. *Nat. Chem.* **2014**, *6*, 575−583.

(23) Alberts, I. L.; Todorov, N. P.; Dean, P. M. Receptor Flexibility in De Novo Ligand Design and Docking. *J. Med. Chem.* **2005**, *48*, 6585−6596.

(24) Schmeing, T. M.; Huang, K. S.; Strobel, S. A.; Steitz, T. A. An Induced-Fit Mechanism to Promote Peptide Bond Formation and Exclude Hydrolysis of Peptidyl-Trna. *Nature* **2005**, *438*, 520−524.

(25) Williamson, J. R. Induced Fit in Rna-Protein Recognition. *Nat. Struct. Biol.* **2000**, *7*, 834−837.

(26) Koshland, D. E. The Key−Lock Theory and the Induced Fit Theory. *Angew. Chem., Int. Ed. Engl.* **1995**, *33*, 2375−2378.

(27) Salsbury, F. R., Jr. Molecular Dynamics Simulations of Protein Dynamics and Their Relevance to Drug Discovery. *Curr. Opin. Pharmacol.* **2010**, *10*, 738−744.

(28) Borhani, D. W.; Shaw, D. E. The Future of Molecular Dynamics Simulations in Drug Discovery. *J. Comput.-Aided Mol. Des.* **2012**, *26*, 15−26.

(29) Durrant, J. D.; McCammon, J. A. Molecular Dynamics Simulations and Drug Discovery. *BMC Biol.* **2011**, *9*, 71.

(30) Flick, J.; Tristram, F.; Wenzel, W. Modeling Loop Backbone Flexibility in Receptor-Ligand Docking Simulations. *J. Comput. Chem.* **2012**, *33*, 2504−2515.

(31) Tian, S.; Sun, H. Y.; Pan, P. C.; Li, D.; Zhen, X. C.; Li, Y. Y.; Hou, T. J. Assessing an Ensemble Docking-Based Virtual Screening Strategy for Kinase Targets by Considering Protein Flexibility. *J. Chem. Inf. Model.* **2014**, *54*, 2664−2679.

(32) Craig, I. R.; Essex, J. W.; Spiegel, K. Ensemble Docking into Multiple Crystallographically Derived Protein Structures: An Evaluation Based on the Statistical Analysis of Enrichments. *J. Chem. Inf. Model.* **2010**, *50*, 511−524.

(33) Huang, S. Y.; Zou, X. Q. Ensemble Docking of Multiple Protein Structures: Considering Protein Structural Variations in Molecular Docking. *Proteins: Struct., Funct., Genet.* **2007**, *66*, 399−421.

(34) Li, Y.; Kim, D. J.; Ma, W. Y.; Lubet, R. A.; Bode, A. M.; Dong, Z. G. Discovery of Novel Checkpoint Kinase 1 Inhibitors by Virtual Screening Based on Multiple Crystal Structures. *J. Chem. Inf. Model.* **2011**, *51*, 2904−2914.

(35) Mahasenan, K. V.; Li, C. L. Novel Inhibitor Discovery through Virtual Screening against Multiple Protein Conformations Generated Via Ligand-Directed Modeling: A Maternal Embryonic Leucine Zipper Kinase Example. *J. Chem. Inf. Model.* **2012**, *52*, 1345−1355.

(36) Wang, L.; Gu, Q.; Zheng, X. H.; Ye, J. M.; Liu, Z. H.; Li, J. B.; Hu, X. P.; Hagler, A.; Xu, J. Discovery of New Selective Human Aldose Reductase Inhibitors through Virtual Screening Multiple Binding Pocket Conformations. *J. Chem. Inf. Model.* **2013**, *53*, 2409−2422.

(37) Tian, S.; Sun, H. Y.; Li, Y. Y.; Pan, P. C.; Li, D.; Hou, T. J. Development and Evaluation of an Integrated Virtual Screening Strategy by Combining Molecular Docking and Pharmacophore Searching Based on Multiple Protein Structures. *J. Chem. Inf. Model.* **2013**, *53*, 2743−2756.

(38) Korb, O.; Olsson, T. S. G.; Bowden, S. J.; Hall, R. J.; Verdonk, M. L.; Liebeschuetz, J. W.; Cole, J. C. Potential and Limitations of Ensemble Docking. *J. Chem. Inf. Model.* **2012**, *52*, 1262−1274.

(39) Alonso, A.; Sasin, J.; Bottini, N.; Friedberg, I.; Osterman, A.; Godzik, A.; Hunter, T.; Dixon, J.; Mustelin, T. Protein Tyrosine Phosphatases in the Human Genome. *Cell* **2004**, *117*, 699−711.

(40) Bottini, N.; Peterson, E. J. Tyrosine Phosphatase Ptpn22: Multifunctional Regulator of Immune Signaling, Development, and Disease. *Annu. Rev. Immunol.* **2014**, *32*, 83−119.

(41) Bottini, N.; Musumeci, L.; Alonso, A.; Rahmouni, S.; Nika, K.; Rostamkhani, M.; MacMurray, J.; Meloni, G. F.; Lucarelli, P.; Pellecchia, M.; Eisenbarth, G. S.; Comings, D.; Mustelin, T. A Functional Variant of Lymphoid Tyrosine Phosphatase Is Associated with Type I Diabetes. *Nat. Genet.* **2004**, *36*, 337−338.

(42) Vang, T.; Liu, W. H.; Delacroix, L.; Wu, S.; Vasile, S.; Dahl, R.; Yang, L.; Musumeci, L.; Francis, D.; Landskron, J.; Tasken, K.; Tremblay, M. L.; Lie, B. A.; Page, R.; Mustelin, T.; Rahmouni, S.; Rickert, R. C.; Tautz, L. Lyp Inhibits T-Cell Activation When Dissociated from Csk. *Nat. Chem. Biol.* **2012**, *8*, 437−446.

(43) Hou, X. B.; Li, R.; Li, K. S.; Yu, X.; Sun, J. P.; Fang, H. Fast Identification of Novel Lymphoid Tyrosine Phosphatase Inhibitors Using Target-Ligand Interaction-Based Virtual Screening. *J. Med. Chem.* **2014**, *57*, 9309−9322.

(44) Vang, T.; Congia, M.; Macis, M. D.; Musumeci, L.; Orru, V.; Zavattari, P.; Nika, K.; Tautz, L.; Tasken, K.; Cucca, F.; Mustelin, T.; Bottini, N. Autoimmune-Associated Lymphoid Tyrosine Phosphatase Is a Gain-of-Function Variant. *Nat. Genet.* **2005**, *37*, 1317−1319.

(45) He, Y. T.; Liu, S. J.; Menon, A.; Stanford, S.; Oppong, E.; Gunawan, A. M.; Wu, L.; Wu, D. J.; Barrios, A. M.; Bottini, N.; Cato, A. C. B.; Zhang, Z. Y. A Potent and Selective Small-Molecule Inhibitor for the Lymphoid-Specific Tyrosine Phosphatase (Lyp), a Target Associated with Autoimmune Diseases. *J. Med. Chem.* **2013**, *56*, 4990−5008.

(46) Yu, X.; Sun, J. P.; He, Y. T.; Guo, X. L.; Liu, S. J.; Zhou, B.; Hudmon, A.; Zhang, Z. Y. Structure, Inhibitor, and Regulatory Mechanism of Lyp, a Lymphoid-Specific Tyrosine Phosphatase Implicated in Autoimmune Diseases. *Proc. Natl. Acad. Sci. U. S. A.* **2007**, *104*, 19767−19772.

(47) Liu, G.; Xin, Z. L.; Liang, H.; Abad-Zapatero, C.; Hajduk, P. J.; Janowick, D. A.; Szczepankiewicz, B. G.; Pei, Z. H.; Hutchins, C. W.; Ballaron, S. J.; Stashko, M. A.; Lubben, T. H.; Berg, C. E.; Rondinone, C. M.; Trevillyan, J. M.; Jirousek, M. R. Selective Protein Tyrosine Phosphatase 1b Inhibitors: Targeting the Second Phosphotyrosine Binding Site with Non-Carboxylic Acid-Containing Ligands. *J. Med. Chem.* **2003**, *46*, 3437−3440.

(48) Sheriff, S.; Beno, B. R.; Zhai, W. X.; Kostich, W. A.; McDonnell, P. A.; Kish, K.; Goldfarb, V.; Gao, M. A.; Kiefer, S. E.; Yanchunas, J.; Huang, Y. L.; Shi, S. H.; Zhu, S. R.; Dzierba, C.; Bronson, J.; Macor, J. E.; Appiah, K. K.; Westphal, R. S.; O'Connell, J.; Gerritz, S. W. Small Molecule Receptor Protein Tyrosine Phosphatase Gamma (Rptp Gamma) Ligands That Inhibit Phosphatase Activity Via Perturbation of the Tryptophan-Proline-Aspartate (Wpd) Loop. *J. Med. Chem.* **2011**, *54*, 6548−6562.

(49) Cui, W.; Cheng, Y. H.; Geng, L. L.; Liang, D. S.; Hou, T. J.; Ji, M. J. Unraveling the Allosteric Inhibition Mechanism of Ptp1b by Free Energy Calculation Based on Umbrella Sampling. *J. Chem. Inf. Model.* **2013**, *53*, 1157−1167.

(50) Wu, S. D.; Bottini, M.; Rickert, R. C.; Mustelin, T.; Tautz, L. In Silico Screening for Ptpn22 Inhibitors: Active Hits from an Inactive Phosphatase Conformation. *ChemMedChem* **2009**, *4*, 440−444.

(51) Barril, X.; Morley, S. D. Unveiling the Full Potential of Flexible Receptor Docking Using Multiple Crystallographic Structures. *J. Med. Chem.* **2005**, *48*, 4432−4443.

(52) Rueda, M.; Bottegoni, G.; Abagyan, R. Recipes for the Selection of Experimental Protein Conformations for Virtual Screening. *J. Chem. Inf. Model.* **2010**, *50*, 186−193.

(53) Venkatraman, V.; Perez-Nueno, V. I.; Mavridis, L.; Ritchie, D. W. Comprehensive Comparison of Ligand-Based Virtual Screening Tools against the Dud Data Set Reveals Limitations of Current 3d Methods. *J. Chem. Inf. Model.* **2010**, *50*, 2079−2093.

(54) Mysinger, M. M.; Carchia, M.; Irwin, J. J.; Shoichet, B. K. Directory of Useful Decoys, Enhanced (Dud-E): Better Ligands and Decoys for Better Benchmarking. *J. Med. Chem.* **2012**, *55*, 6582−6594.

(55) Kao, R. Y. T.; Jenkins, J. L.; Olson, K. A.; Key, M. E.; Fett, J. W.; Shapiro, R. A Small-Molecule Inhibitor of the Ribonucleolytic Activity of Human Angiogenin That Possesses Antitumor Activity. *Proc. Natl. Acad. Sci. U. S. A.* **2002**, *99*, 10066−10071.

(56) Jenkins, J. L.; Kao, R. Y. T.; Shapiro, R. Virtual Screening to Enrich Hit Lists from High-Throughput Screening: A Case Study on Small-Molecule Inhibitors of Angiogenin. *Proteins: Struct., Funct., Genet.* **2003**, *50*, 81−93.

(57) Maggiora, G.; Vogt, M.; Stumpfe, D.; Bajorath, J. Molecular Similarity in Medicinal Chemistry. *J. Med. Chem.* **2014**, *57*, 3186−3204.

(58) Salim, N.; Holliday, J.; Willett, P. Combination of Fingerprint-Based Similarity Coefficients Using Data Fusion. *J. Chem. Inf. Model.* **2003**, *43*, 435−442.

(59) Baell, J. B.; Holloway, G. A. New Substructure Filters for Removal of Pan Assay Interference Compounds (Pains) from Screening Libraries and for Their Exclusion in Bioassays. *J. Med. Chem.* **2010**, *53*, 2719−2740.

(60) Dimova, D.; Hu, Y.; Bajorath, J. Matched Molecular Pair Analysis of Small Molecule Microarray Data Identifies Promiscuity Cliffs and Reveals Molecular Origins of Extreme Compound Promiscuity. *J. Med. Chem.* **2012**, *55*, 10220−10228.

(61) Hu, Y.; Bajorath, J. Growth of Ligand-Target Interaction Data in Chembl Is Associated with Increasing and Activity Measurement-Dependent Compound Promiscuity. *J. Chem. Inf. Model.* **2012**, *52*, 2550−2558.

(62) Mendgen, T.; Steuer, C.; Klein, C. D. Privileged Scaffolds or Promiscuous Binders: A Comparative Study on Rhodanines and Related Heterocycles in Medicinal Chemistry. *J. Med. Chem.* **2012**, *55*, 743−753.

(63) Erbe, D. V.; Wang, S.; Zhang, Y. L.; Harding, K.; Kung, L.; Tam, M.; Stolz, L.; Xing, Y.; Furey, S.; Qadri, A.; Klaman, L. D.; Tobin, J. F. Ertiprotafib Improves Glycemic Control and Lowers Lipids Via Multiple Mechanisms. *Mol. Pharmacol.* **2005**, *67*, 69−77.

(64) Cousin, D.; Mann, J.; Nieuwenhuyzen, M.; van den Berg, H. A New Approach to Combretastatin D2. *Org. Biomol. Chem.* **2006**, *4*, 54.

(65) Barr, A. J.; Ugochukwu, E.; Lee, W. H.; King, O. N.; Filippakopoulos, P.; Alfano, I.; Savitsky, P.; Burgess-Brown, N. A.; Muller, S.; Knapp, S. Large-Scale Structural Analysis of the Classical Human Protein Tyrosine Phosphatome. *Cell* **2009**, *136*, 352−363.

(66) Stanford, S. M.; Krishnamurthy, D.; Falk, M. D.; Messina, R.; Debnath, B.; Li, S.; Liu, T.; Kazemi, R.; Dahl, R.; He, Y. T.; Yu, X. A.; Chan, A. C.; Zhang, Z. Y.; Barrios, A. M.; Woods, V. L.; Neamati, N.; Bottini, N. Discovery of a Novel Series of Inhibitors of Lymphoid Tyrosine Phosphatase with Activity in Human T Cells. *J. Med. Chem.* **2011**, *54*, 1640−1654.

(67) Pronk, S.; Pall, S.; Schulz, R.; Larsson, P.; Bjelkmar, P.; Apostolov, R.; Shirts, M. R.; Smith, J. C.; Kasson, P. M.; van der Spoel, D.; Hess, B.; Lindahl, E. Gromacs 4.5: A High-Throughput and Highly Parallel Open Source Molecular Simulation Toolkit. *Bioinformatics* **2013**, *29*, 845−854.

(68) Van der Spoel, D.; Lindahl, E.; Hess, B.; Groenhof, G.; Mark, A. E.; Berendsen, H. J. C. Gromacs: Fast, Flexible, and Free. *J. Comput. Chem.* **2005**, *26*, 1701−1718.

(69) Lindorff-Larsen, K.; Piana, S.; Palmo, K.; Maragakis, P.; Klepeis, J. L.; Dror, R. O.; Shaw, D. E. Improved Side-Chain Torsion Potentials for the Amber Ff99sb Protein Force Field. *Proteins: Struct., Funct., Genet.* **2010**, *78*, 1950−1958.

(70) Mark, P.; Nilsson, L. Structure and Dynamics of the Tip3p, Spc, and Spc/E Water Models at 298 K. *J. Phys. Chem. A* **2001**, *105*, 9954−9960.

(71) Cerutti, D. S.; Duke, R. E.; Darden, T. A.; Lybrand, T. P. Staggered Mesh Ewald: An Extension of the Smooth Particle-Mesh Ewald Method Adding Great Versatility. *J. Chem. Theory Comput.* **2009**, *5*, 2322−2338.

(72) Hess, B. P-Lincs: A Parallel Linear Constraint Solver for Molecular Simulation. *J. Chem. Theory Comput.* **2008**, *4*, 116−122.

(73) Wang, J. M.; Wang, W.; Kollman, P. A.; Case, D. A. Automatic Atom Type and Bond Type Perception in Molecular Mechanical Calculations. *J. Mol. Graphics Modell.* **2006**, *25*, 247−260.

(74) Wang, J. M.; Wolf, R. M.; Caldwell, J. W.; Kollman, P. A.; Case, D. A. Development and Testing of a General Amber Force Field. *J. Comput. Chem.* **2004**, *25*, 1157−1174.

(75) Jakalian, A.; Jack, D. B.; Bayly, C. I. Fast, Efficient Generation of High-Quality Atomic Charges. Am1-Bcc Model: Ii. Parameterization and Validation. *J. Comput. Chem.* **2002**, *23*, 1623−1641.

(76) Jakalian, A.; Bush, B. L.; Jack, D. B.; Bayly, C. I. Fast, Efficient Generation of High-Quality Atomic Charges. Am1-Bcc Model: I. Method. *J. Comput. Chem.* **2000**, *21*, 132−146.

(77) Pettersen, E. F.; Goddard, T. D.; Huang, C. C.; Couch, G. S.; Greenblatt, D. M.; Meng, E. C.; Ferrin, T. E. Ucsf Chimera - a Visualization System for Exploratory Research and Analysis. *J. Comput. Chem.* **2004**, *25*, 1605−1612.

(78) Hou, X.; Du, J.; Liu, R.; Zhou, Y.; Li, M.; Xu, W.; Fang, H. Enhancing the Sensitivity of Pharmacophore-Based Virtual Screening by Incorporating Customized Zbg Features: A Case Study Using Histone Deacetylase 8. *J. Chem. Inf. Model.* **2015**, *55*, 861−871.

(79) Yu, X.; Sun, J. P.; He, Y.; Guo, X.; Liu, S.; Zhou, B.; Hudmon, A.; Zhang, Z. Y. Structure, Inhibitor, and Regulatory Mechanism of Lyp, a Lymphoid-Specific Tyrosine Phosphatase Implicated in Autoimmune Diseases. *Proc. Natl. Acad. Sci. U. S. A.* **2007**, *104*, 19767−19772.

(80) Liu, J.; Chen, M.; Li, R.; Yang, F.; Shi, X.; Zhu, L.; Wang, H. M.; Yao, W.; Liu, Q.; Meng, F. G.; Sun, J. P.; Pang, Q.; Yu, X. Biochemical and Functional Studies of Lymphoid-Specific Tyrosine Phosphatase (Lyp) Variants S201f and R266w. *PLoS One* **2012**, *7*, e43631.

(81) Huijbers, I. J.; Bin Ali, R.; Pritchard, C.; Cozijnsen, M.; Kwon, M. C.; Proost, N.; Song, J. Y.; de Vries, H.; Badhai, J.; Sutherland, K.; Krimpenfort, P.; Michalak, E. M.; Jonkers, J.; Berns, A. Rapid Target Gene Validation in Complex Cancer Mouse Models Using Re-Derived Embryonic Stem Cells. *EMBO Mol. Med.* **2014**, *6*, 212−225.

(82) Gloria-Bottini, F.; Ammendola, M.; Saccucci, P.; Pietropolli, A.; Magrini, A.; Bottini, E. The Association of Ptpn22 Polymorphism with Endometriosis: Effect of Genetic and Clinical Factors. *Eur. J. Obstet. Gynecol. Reprod. Biol.* **2013**, *169*, 60−63.

(83) Pan, C.; Liu, H. D.; Gong, Z.; Yu, X.; Hou, X. B.; Xie, D. D.; Zhu, X. B.; Li, H. W.; Tang, J. Y.; Xu, Y. F.; Yu, J. Q.; Zhang, L. Y.; Fang, H.; Xiao, K. H.; Chen, Y. G.; Wang, J. Y.; Pang, Q.; Chen, W.; Sun, J. P. Cadmium Is a Potent Inhibitor of Ppm Phosphatases and Targets the M1 Binding Site. *Sci. Rep.* **2013**, *3*, 2333.

(84) Sun, J. P.; Fedorov, A. A.; Lee, S. Y.; Guo, X. L.; Shen, K.; Lawrence, D. S.; Almo, S. C.; Zhang, Z. Y. Crystal Structure of Ptp1b Complexed with a Potent and Selective Bidentate Inhibitor. *J. Biol. Chem.* **2003**, *278*, 12406−12414.